Phytochemistry 111 (2015) 37–47

Contents lists available at ScienceDirect

Phytochemistry

journal homepage: www.elsevier.com/locate/phytochem

# Allosteric substrate inhibition of Arabidopsis NAD-dependent malic enzyme 1 is released by fumarate

Marcos Ariel Tronconi *, Mariel Claudia Gerrard Wheeler, Andrea Martinatto, Juan Pablo Zubimendi, Carlos Santiago Andreo, María Fabiana Drincovich

*Centro de Estudios Fotosintéticos y Bioquímicos (CEFOBI), Facultad de Ciencias Bioquímicas y Farmacéuticas, Universidad Nacional de Rosario, Suipacha 531, 2000 Rosario, Argentina*

ARTICLE INFO

*Article history:*
Received 13 June 2014
Received in revised form 21 October 2014
Available online 26 November 2014

*Keywords:*
*Arabidopsis thaliana*
Cruciferae
Regulatory site
Mitochondria
Malic enzyme
L-Malate
Fumarate

ABSTRACT

Plant mitochondria can use L-malate and fumarate, which accumulate in large levels, as respiratory substrates. In part, this property is due to the presence of NAD-dependent malic enzymes (NAD-ME) with particular biochemical characteristics. Arabidopsis NAD-ME1 exhibits a non-hyperbolic behavior for the substrate L-malate, and its activity is strongly stimulated by fumarate. Here, the possible structural connection between these properties was explored through mutagenesis, kinetics, and fluorescence studies. The results indicated that NAD-ME1 has a regulatory site for L-malate that can also bind fumarate. L-Malate binding to this site elicits a sigmoidal and low substrate-affinity response, whereas fumarate binding turns NAD-ME1 into a hyperbolic and high substrate affinity enzyme. This effect was also observed when the allosteric site was either removed or altered. Hence, fumarate is not really an activator, but suppresses the inhibitory effect of L-malate. In addition, residues Arg50, Arg80 and Arg84 showed different roles in organic acid binding. These residues form a triad, which is the basis of the homo and heterotrophic effects that characterize NAD-ME1. The binding of L-malate and fumarate at the same allosteric site is herein reported for a malic enzyme and clearly indicates an important role of NAD-ME1 in processes that control flow of $C_4$ organic acids in Arabidopsis mitochondrial metabolism.



## 1. Introduction

Eukaryotic cells possess a mitochondrial NAD-dependent malic enzyme (mNAD-ME) that catalyzes the oxidative decarboxylation of L-malate to yield pyruvate and $CO_2$, with $NAD^+$ and a divalent metal ion ($Mn^{+2}$ or $Mg^{+2}$) being essential cofactors for the reaction. Despite having the same sub-cellular location, animal (EC 1.1.1.38) and plant (EC 1.1.1.39) mNAD-MEs differ in kinetic and structural features. For example, animal and plant mNAD-MEs are classified into different groups on the basis of their ability, or lack thereof, to decarboxylate oxaloacetate. In addition, animal enzymes are capable of catalyzing the reverse reaction (reductive pyruvate carboxylation) considerably, although this activity is not significant in botanic isoforms (Mallick et al., 1991; Tronconi et al., 2010a). More interestingly, whereas animal mNAD-MEs are assembled as tetramers of identical subunits, plant orthologs have been purified from different tissues as hetero-oligomers composed of two dissimilar subunits (Willeford and Wedding, 1987). The biochemical differences of mNAD-MEs from unrelated organisms are not surprising if one takes into account the specificity of function that these enzymes have shown in each case (Hanning and Heldt, 1993; Jiang et al., 2013; Moreadith and Lehninger, 1984; Rao et al., 2003; Tronconi et al., 2008).

In plants, mNAD-ME occupies a key position in the central pathways of carbon metabolism. The large reserves of L-malate commonly present in many species can be used, thanks to mNAD-ME activity, as the substrate for the tricarboxylic acid cycle (TCA), replacing the imported cytosolic pyruvate (Sweetlove et al., 2010). This scenario diminishes the dependence of TCA on glycolysis, providing an advantage in terms of metabolic flexibility that is critical for organisms with a sessile lifestyle. Recently, a comprehensive analysis of *Arabidopsis thaliana* mNAD-ME established novel properties for this enzyme (Tronconi et al., 2012, 2010a,b, 2008). The genome of this $C_3$ species contains two nuclear genes encoding mNAD-ME (*NAD-ME1*, TAIR: AT2g13560 and *NAD-ME2*, TAIR: AT4g00570). The encoded proteins (NAD-ME1 and NAD-ME2) can form two separate active homodimers, as well as a heterodimer (NAD-MEH) *in vitro* and *in vivo* (Tronconi et al., 2010b, 2008). Though *NAD-ME1* and *-2* show similar expression patterns in mature organs of Arabidopsis, both proteins accumulate at different levels in the separate components of inflorescences (Tronconi et al., 2010b, 2008). In leaves, both homo-dimers and

* Corresponding author. Tel.: +54-341-4371955; fax: +54-341-4370044.
*E-mail address:* tronconi@cefobi-conicet.gov.ar (M.A. Tronconi).

http://dx.doi.org/10.1016/j.phytochem.2014.11.009
0031-9422/

the hetero-dimer would be acting in concert and the characterization of an Arabidopsis mutant plants lacking mNAD-ME activity indicated a major participation of these isoforms in nocturnal L-malate oxidation, as well as in the coordination of carbon and nitrogen metabolism (Tronconi et al., 2008).

Recombinant NAD-ME1 and -2 homodimers possess particular kinetic and regulatory properties. They behave differently in terms of catalytic mechanism and interaction with the substrates (Tronconi et al., 2010a). While NAD-ME2 exhibits hyperbolic kinetics with respect to L-malate, NAD-ME1 shows a marked sigmoidicity, which would indicate either cooperativity between active sites in the dimer or the existence of an allosteric site for L-malate on the surface of NAD-ME1. Also, both isoforms differ in their regulation by effectors. NAD-ME1 activity is strongly enhanced by $C_4$ organic acids, especially fumarate, which binds at an allosteric site present in this enzyme (Tronconi et al., 2012). In contrast, this acid acts as inhibitor of NAD-ME2 activity (Tronconi et al., 2010b). The biochemical characterization of mutants and chimeric proteins of NAD-ME1 and -2 indicated that the amino-terminal region of NAD-ME1 is implicated in fumarate activation and sigmoidal L-malate responses (Tronconi et al., 2012, 2010b). In this work, the possible structural connection was explored between these two properties. Site-directed mutagenesis was used in combination with detailed kinetic analysis and fluorescence studies. When taken together, the results obtained indicated that NAD-ME1 exhibits a complex homo and heterotrophic allosteric regulation with L-malate wielding an inhibitory effect that is cancelled by competitive fumarate binding. This type of regulation is reported for the first time for a malic enzyme and its physiological significance in relation to plant metabolism is discussed.

## 2. Results

### *2.1. Kinetic behavior for L-Malate of NAD-ME1, -2 and two chimeric proteins in the presence of fumarate*

In the absence of fumarate, NAD-ME1 presents a sigmoidal kinetic response for L-malate ($n_H$ = 1.9; Fig. 1A), while NAD-ME2 shows a typical hyperbolic behavior (Fig. 1B) (Tronconi et al., 2010a). Here, the response to increasing fumarate concentrations

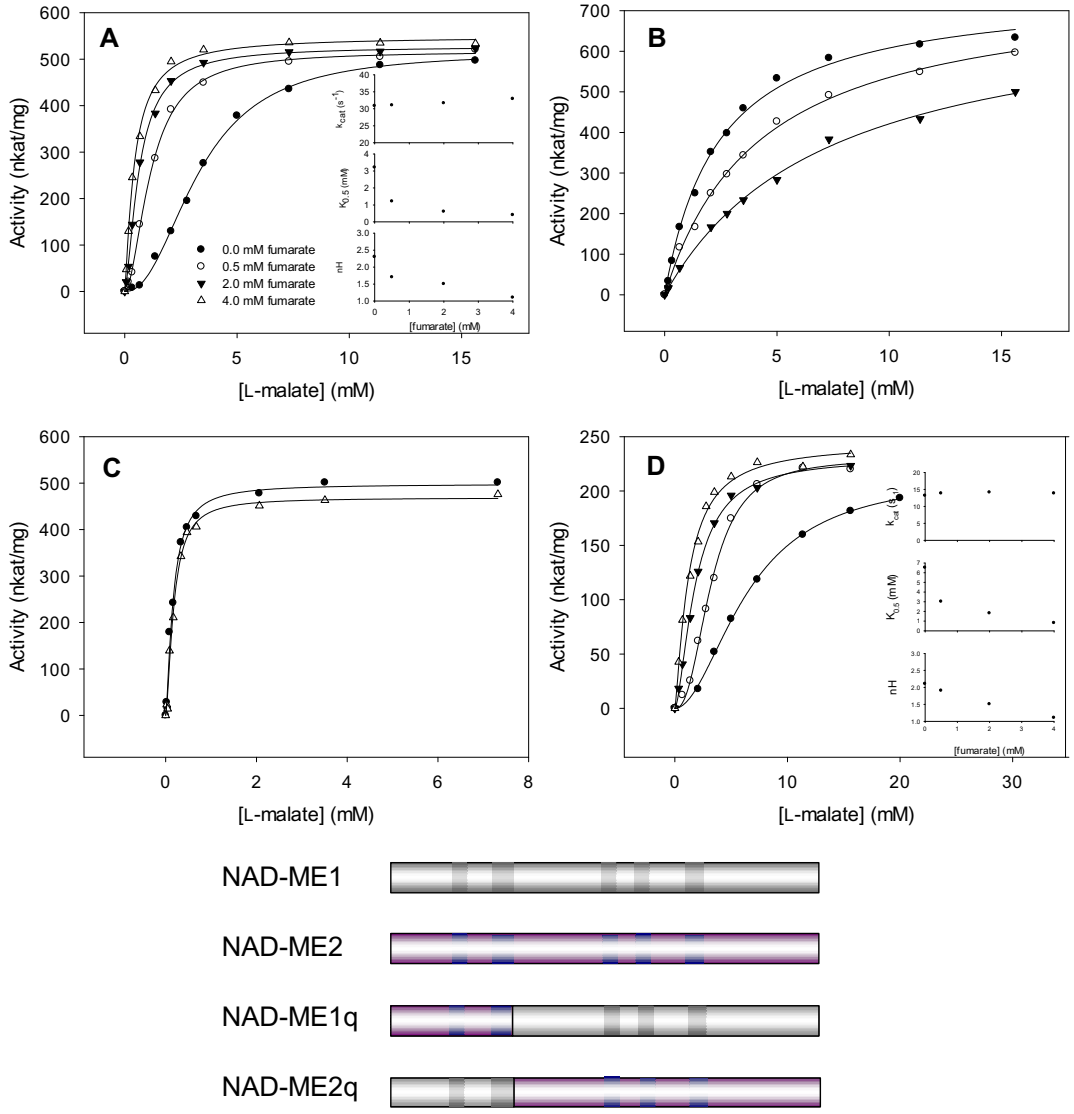


**Fig. 1.** Effect of fumarate on L-malate kinetic behavior of NAD-ME1 (A), NAD-ME2 (B), NAD-ME1q (C) and NAD-ME2q (D). Typical results from at least three independent determinations are shown. Assays were done at 4 mM NAD and 10 mM $MnCl_2$ in the presence of the indicated fumarate concentrations. For NAD-ME1 and -2q, $k_{cat}$, $K_{0.5}$ for L-malate and $n_H$ as function of fumarate concentration are shown as inset. The estimated $K_{0.5}$ for L-malate, $n_H$ and $k_{cat}$ of each enzyme in the presence of 4 mM fumarate are indicated in Table 1.

**Table 1**
Kinetic properties of wild-type, chimeric and mutant Arabidopsis NAD-MEs. The indicated values are the average of at least three different experiments with no more than 5% S.D. among them. The $K_{0.5}$ and $k_{cat}$ values are expressed in mM and $sec^{-1}$, respectively.

| | No fumarate added | | | With 4 mM fumarate | | |
|---|---|---|---|---|---|---|
| | $K_{0.5}$ L-malate | $k_{cat}$ | $k_{cat}/K_{0.5}$ | $K_{0.5}$ L-malate | $k_{cat}$ | $k_{cat}/K_{0.5}$ |
| NAD-ME1 | 3.0[a] (1.9)[b] | 31.1[a] | 10.4 | 0.4 (1.1)[b] | 32.9 | 82.3 |
| NAD-ME2 | 3.0[a] | 44.1[a] | 14.7 | 7.2 | 43.6 | 6.1 |
| NAD-ME1q | 0.2[a] | 32.1[a] | 160.5 | NM | NM | NM |
| NAD-ME2q | 6.5[c] (2.1)[b] | 11.4[a] | 1.8 | 0.8 (1.1)[b] | 13.8 | 17.3 |
| NAD-ME1R50A | 0.4 | 27.5 | 68.8 | NM | NM | NM |
| NAD-ME1R80A | 0.6 | 29.0 | 48.3 | 0.4 | 31.4 | 78.5 |
| NAD-ME1R84A | 3.2[a] | 28.7[a] | 9.0 | NM | NM | NM |

[a] Values previously obtained (Tronconi et al., 2012, 2010b, 2008) are included for comparison.
[b] $K_{0.5}$; the calculated Hill coefficient ($n_H$) is indicated in parentheses.
[c] Value was corrected to previously specified (Tronconi et al., 2010b) according to the results obtained for new purifications of this enzyme. NM: not modified.

on L-malate saturation curves for both enzymes was evaluated. In NAD-ME1, fumarate acts as activator (Tronconi et al., 2010b) and an increase in its concentration produces a drastic decrease in the $n_H$ and $K_{0.5}$ values of L-malate (Fig. 1A). At 4 mM fumarate, the NAD-ME1 kinetic behavior was almost hyperbolic ($n_H = 1.1$) with a $K_{0.5}$ 7.5-fold lower than for the enzyme in the absence of activator (Table 1). The presence of fumarate did not produce significant modifications in $k_{cat}$ value (Fig. 1A). Thus, NAD-ME1 catalytic efficiency is increased about 8-fold by 4 mM fumarate (Table 1). On the other hand, this acid decreases NAD-ME2 activity by binding to the L-malate position in the active site (Fig. 1B; Tronconi et al., 2012), which results in a 2-fold decrease of NAD-ME2 catalytic efficiency in the presence of fumarate (Table 1).

The characterization of two chimeric proteins between NAD-ME1 and -2 indicated that the amino-terminal region of both isoforms is associated with the differences in the response to L-malate and fumarate (Tronconi et al., 2010a,b). NAD-ME1q chimeric protein, which is composed of the first 176 amino acid residues of NAD-ME2 and the central and C-terminal sequence of NAD-ME1 (Fig. 1), exhibits a significantly lower $K_{0.5}$ L-malate value than the parental isoforms (Table 1) and a hyperbolic behavior that is not modified by fumarate (Fig. 1C; Tronconi et al., 2010b). On the other hand, NAD-ME2q chimeric protein, that possesses the first 176 amino acid residues of NAD-ME1 and the central and C-terminal sequence of NAD-ME2 (Fig. 1), presents a sigmoidal L-malate response similar to the one for NAD-ME1 (Fig. 1D; Tronconi et al., 2010b), but also a higher $K_{0.5}$ L-malate value and a lower $k_{cat}$ value (Table 1). NAD-ME2q is activated by fumarate (Tronconi et al., 2010b) and an increase in its concentration produced a decrease in $K_{0.5}$ and $n_H$ values (Fig. 1D). At 4 mM fumarate, the L-malate saturation curve was hyperbolic ($n_H = 1.1$) with an 8-fold decrease in $K_{0.5}$ value (Table 1). There were no significant changes in $k_{cat}$ value by addition of fumarate (Fig. 1D), which implies a 9-fold increase in NAD-ME2q catalytic efficiency when compared to the enzyme in the absence of fumarate (Table 1).

### 2.2. L-Malate as quencher of the fluorescence of tryptophan residues

To determine whether L-malate binds to more than one site in NAD-ME1, a fluorescence titration assay with L-malate was carried out. When the NAD-ME1 quenching data were expressed according to the Stern–Volmer (S–V) equation (Eq. (1)), both proteins showed curvilinear responses (Suppl. Fig. 1). This indicated that there is a heterogeneous population of tryptophan residues differing in their capacity to be quenched by L-malate (Tronconi et al., 2012). Thus,

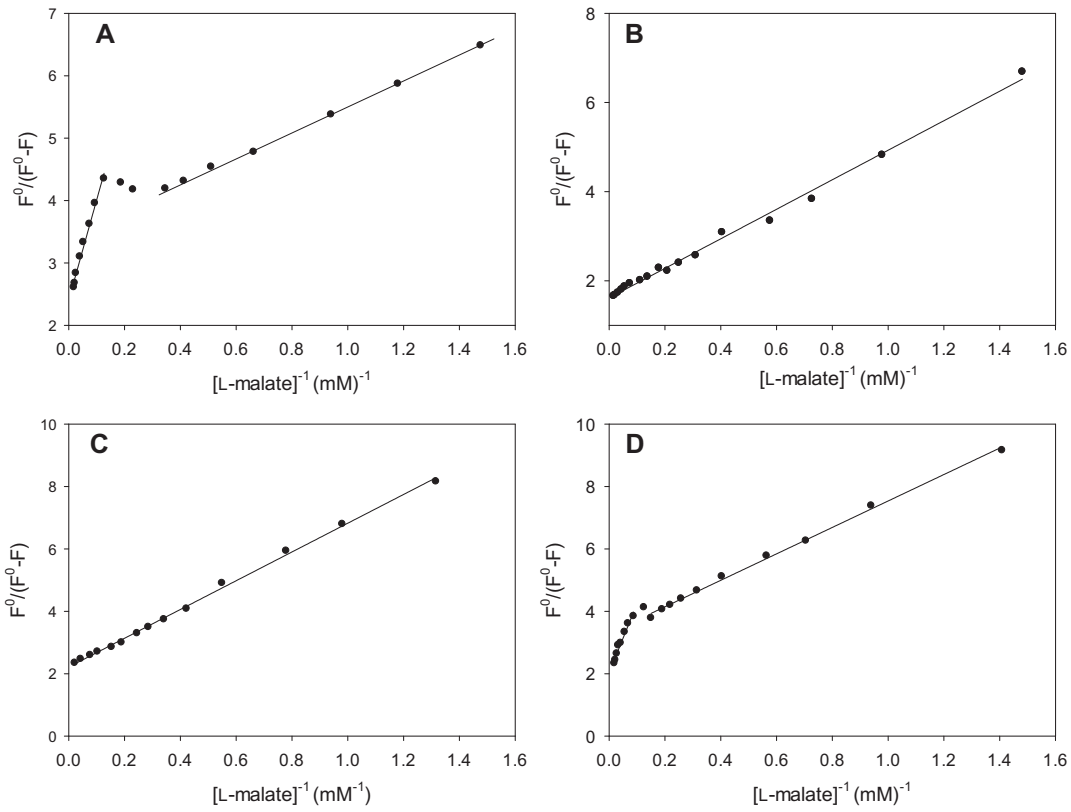


**Fig. 2.** Fluorescence titration by L-malate. Modified Stern–Volmer representation of quenching data for NAD-ME1 (A), NAD-ME2 (B), NAD-ME1q (C) and NAD-ME2q (D) are shown. The excitation wavelength was set at 295 nm and the fluorescence was recorded at 344 nm. All values were corrected for buffer spectra and dilution. The quenching constants are summarized in Table 2.

the data were analyzed in terms of the modified S–V equation (Eq. (2)). For NAD-ME2, data representation was linear giving a value of $K = 0.1\ mM^{-1}$ (Fig. 2B). This value is about 10-fold higher than the $K_d$ value obtained for dynamic quenching of free tryptophan by L-malate ($K_d = 0.009\ mM^{-1}$, Fig. 2E). This result suggests that L-malate quenches NAD-ME2 fluorescence by a static process that implicates substrate binding to one site in the enzyme. Then, the $K_D$ value for the L-malate-enzyme complex was 10 mM (Table 2), which would correspond to the affinity of L-malate to NAD-ME2 active site in the absence of substrate NAD. This low affinity of L-malate to the active site is not surprising, as this isoform exhibits a sequential ordered Bi-Ter mechanism, with NAD being the leading substrate (Tronconi et al., 2010a).

For NAD-ME1, S–V representation of quenching data provided a biphasic curve (Suppl. Fig. 1). The modified S–V plot of data resulted in two linear segments that allowed the estimation of two $K$ values (Fig. 2A), which were significantly higher than the $K_d$ for free tryptophan quenching (Suppl. Fig. 1E). Alternatively, Stern–Volmer data quenching were fit to a sum of two binding isotherms (Eq. (4)). The square residues from this fit were lower than those obtained by fitting to a single binding isotherm (Eq. (3)) and the estimated $K$ values were no more than 10% different from those calculated using the modified S–V equation (data not shown). These results are consistent with L-malate binding to two sites which differ in their affinity for the substrate in NAD-ME1. Thus, the $K_D$ values were 0.4 mM ($K_{D1}$) and 11 mM ($K_{D2}$), for the first and the second semi-curve of S–V plot, respectively (Suppl. Fig. 1, Table 2). Taking into account the $K_D$ obtained for NAD-ME2, and the fact that NAD-ME1 and -2 homodimers present similar $K_{0.5}$ values for L-malate (Table 2), it can be suggested that $K_{D2}$ is the dissociation constant of L-malate from the active site of NAD-ME1 in the absence of NAD (Table 2). Thereby, $K_{D1}$ may represent L-malate affinity for an exosite exclusively present in NAD-ME1 (Table 2).

NAD-ME1q and -2 chimeric proteins were also analyzed by L-malate fluorescence quenching assays. For NAD-ME1q, the S–V data representation exhibited a single-phase curvilinear response (Suppl. Fig. 1), resulting in a linear modified S–V plot (Fig. 2C) with a $K_D$ value for substrate-enzyme complex of 3 mM (Table 2). On the other hand, NAD-ME2q quenching showed a biphasic S–V curve (Suppl. Figure 1). The $K_{D1}$ and $K_{D2}$ values obtained from the two linear segments of the modified S–V equation (Fig. 2D) were 0.6 mM and 18 mM, respectively (Table 2). The results indicate that the L-malate exosite was either lost or gained by the amino-terminal sequence replacements in NAD-ME1q and -2q, respectively.

### 2.3. Competition assays

NAD-ME1 presents an allosteric site for fumarate which regulates its activation by this metabolite (Tronconi et al., 2012). Thus, fumarate quenches NAD-ME1 fluorescence by binding to this site with a $K_D = 1.4$ mM (Tronconi et al., 2012). However, in the presence of 15 mM L-malate, the $K_D$ for fumarate was 2.5 mM (Fig. 3A), which implies that the NAD-ME1 fumarate affinity is decreased by this substrate. The converse experiment in which the NAD-ME1 fluorescence was quenched by L-malate in the presence of 4 mM fumarate was also performed. In this case, S–V data representation resulted in a linear graph, instead of the biphasic curve exhibited in the absence of the activator (Fig. 3B). In this regard, the $K_D$ value for L-malate in the presence of 4 mM fumarate was 1.5 mM, a value 7-fold lower than the one observed without effector (Table 2). Hence, fumarate and L-malate compete for the binding to NAD-ME1, indicating that the substrate also binds to the previously characterized allosteric site.

### 2.4. Site-directed mutagenesis studies of L-Malate and fumarate binding to NAD-ME1 allosteric site

In recent work, Arg84 of NAD-ME1 was shown to be essential for fumarate activation (Tronconi et al., 2012). Residues homologous to Arg84 have been implicated in fumarate activation of mitochondrial NAD(P)-ME from human (Yang et al., 2002), *Ascaris suum* (Karsten et al., 2003) and NADP-ME2 from *A. thaliana* (Arias et al., 2013) (Fig. 4A). The replacement of Arg84 by Ala in NAD-ME1

**Table 2**
L-Malate dissociation constants for wild-type, chimeric and mutant Arabidopsis NAD-MEs The fluorescence decrease by different L-malate concentrations was analyzed by Stern–Volmer plots. In the cases of biphasic curves, $K_{D1}$ and $K_{D2}$ correspond to the first and the second semi-curve, respectively. The indicated values are the average of at least two different quenching experiments with no more than 5% S.D. among them. The values are expressed in mM.

| | NAD-ME1 | NAD-ME2 | NAD-ME1q | NAD-ME2q | ME1R50A | ME1R80A | ME1R84A |
|---|---|---|---|---|---|---|---|
| $K_{D1}$ | 0.4 | – | – | 0.6 | – | – | 2 |
| $K_{D2}$ | 11 | 10 | 3 | 18 | 5 | 6 | 10 |

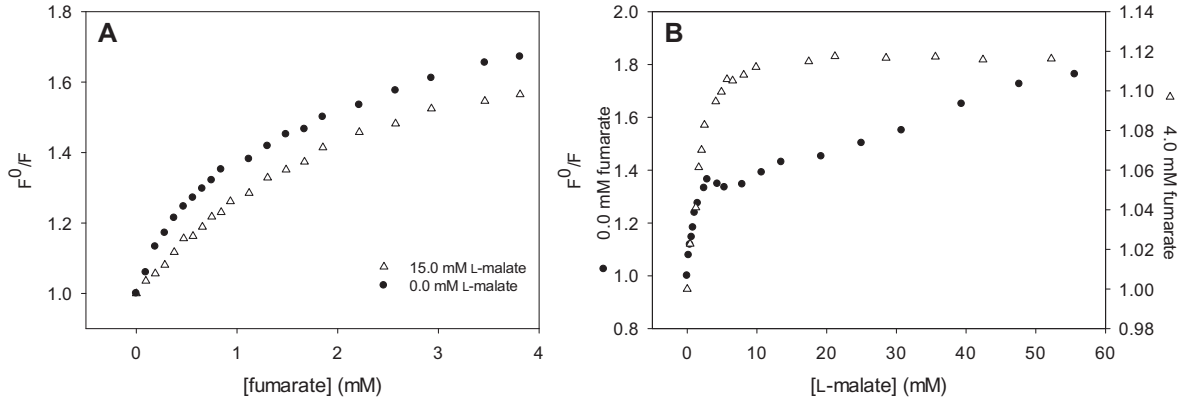


**Fig. 3.** Competition assays. Stern–Volmer representation of NAD-ME1 fluorescence quenching by fumarate in the presence of 15 mM L-malate (A) and NAD-ME1 fluorescence quenching by L-malate in the presence of 4 mM fumarate (B). The excitation wavelength was set at 295 nm and the fluorescence was recorded at 344 nm. All values were corrected for buffer spectra and dilution.

resulted in a mutant protein (NAD-ME1R84A) that could not bind fumarate at the allosteric site, as it presented collisional quenching by this metabolite (Tronconi et al., 2012). Here, NAD-ME1R84A protein was further characterized regarding its kinetic properties. The mutant protein showed $K_{0.5}$ values for L-malate and $NAD^+$ that were similar to the wild-type enzyme $K_{0.5}$ values (Tronconi et al., 2012), and with no changes in $k_{cat}$ values (Table 1). More interestingly, the L-malate kinetic behavior for this mutant was hyperbolic, instead of sigmoidal as was shown for NAD-ME1 (Fig. 5A). Fluorescence quenching by L-malate performed on R84A protein resulted in a modified S–V plot with two linear segments, as in NAD-ME1 (Fig. 5B). However, while the $K_{D2}$ value for the mutant was similar to the one observed for the wild-type enzyme, its $K_{D1}$ value was 5-fold higher (Table 2). Thus, the affinity of L-malate for the exosite was decreased by R84A mutation.

The roles of other Arg residues in $C_4$ organic acid binding at the allosteric site of NAD-ME1 were analyzed. In this isoform, Arg50 is homologous to Arg67 and Arg81 from human and *A. suum* NAD-ME, respectively (Fig. 4A), which are ligands for fumarate binding (Rao et al., 2003; Yang et al., 2002). In this work, NAD-ME1R50A mutant protein was generated and characterized. The mutation introduced had no significant effect on the kinetics for NAD (data not shown), with a $K_{0.5}$ value equal to that of the parental enzyme (0.5 mM) (Tronconi et al., 2008). However, NAD-ME1R50A kinetic behavior for L-malate was hyperbolic (Fig. 5A) with a $K_{0.5}$ value 7-fold lower than that of the wild-type enzyme (Table 1). The $k_{cat}$ was only slightly decreased in the mutant enzyme when compared to NAD-ME1 (Table 1). Furthermore, NAD-MER50A was not activated by fumarate (Suppl. Fig. 2A). Moreover, fluorescence assays using fumarate as a quencher showed that the mutant exhibits dynamic quenching by this acid (Suppl. Fig. 2B), which indicates that the mutation abolishes fumarate binding at the allosteric site. When L-malate was used as quencher, a single-phase linear modified S–V plot was obtained (Fig. 5B) with a $K_D$ value of 5 mM (Table 2). This result suggests that the Arg50 replacement performed on NAD-ME1 also avoids L-malate binding to the allosteric site.

In addition, the predicted three dimensional model of NAD-ME1 using *A. suum* mNAD-ME as template suggested that another Arg residue, Arg80, could be interacting with fumarate (Fig. 4B). This residue is not present in the human and *A. suum* isoforms (Fig. 4A). Thus, to analyze the role of Arg80 at $C_4$ organic acid allosteric site, this residue was changed by Ala in NAD-ME1. The mutant NAD-ME1R80A showed a hyperbolic L-malate response (Fig. 5A) with an increase of 5-fold in the catalytic efficiency compared to NAD-ME1, due to a decrease in the $K_{0.5}$ value (Table 1). It is worth mentioning that the $K_{0.5}$ for NAD was not modified by the replacement (data not shown). This mutant protein was activated by fumarate, although to lesser extent (Suppl. Fig. 2A). In this regard, the catalytic efficiency ratio with and without this metabolite was 1.6 for R80A compared to 7.9 for the parental enzyme (data from Table 1). The $K_D$ value for fumarate estimated by fluorescence quenching assays indicated that the mutation does not significantly modify fumarate affinity for the allosteric site (Suppl. Fig. 2B). When L-malate was used as quencher, a single-phase linear modified S–V plot was obtained (Fig. 5B) with a $K_D$ value of

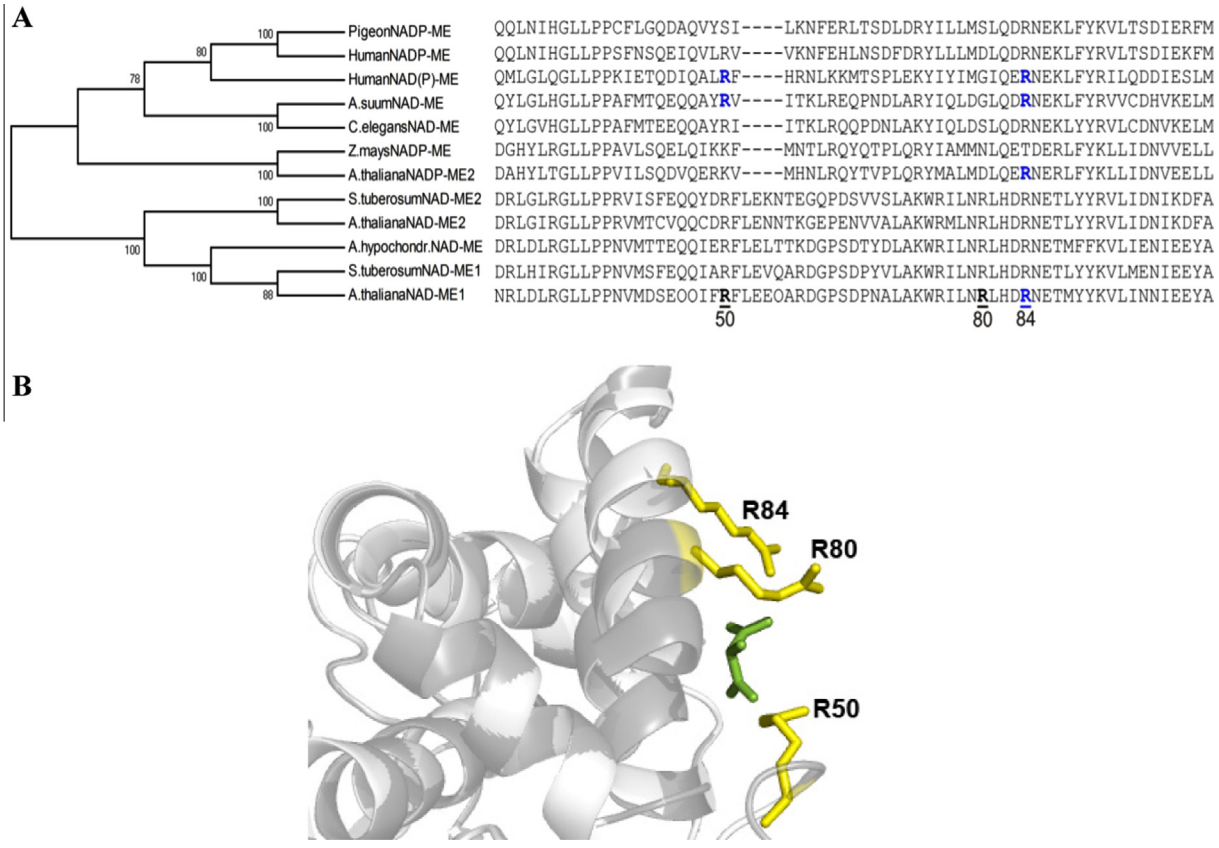


**Fig. 4.** Sequence alignment and predicted structure of NAD-ME1. (A) Multiple sequence alignment of the amino terminal end of several NAD (P)-ME isoforms. The amino acid residues highlighted in blue have been identified by site-directed mutagenesis to be involved in the activation by fumarate (Gerrard Wheeler et al., 2008; Karsten et al., 2003; Tronconi et al., 2012; Yang et al., 2002). The residues that were analyzed in this work are underlined. The numbers below sequences refer to their position in NAD-ME1. (B) Three-dimensional model view of NAD-ME1. The predicted model was obtained with the protein structure homology-modeling server (SWISS-MODEL; http://expasy.ch/swissmod/SWISS-MODEL.html) using *A. suum* NAD-ME complexed with a fumarate analog (tartronate) and NAD as template (Rao et al., 2003). The figure was created by using Swiss PDB Viewer version 3.7. The position of Arg50, Arg80 and Arg84 are indicated in yellow. Tartronate in the allosteric site is showed in green. (For interpretation of the references to color in this figure legend, the reader is referred to the web version of this article.)

6 mM (Table 2). This suggests that the Arg80 replacement performed on NAD-ME1 abolishes L-malate but not fumarate binding at the allosteric site.

### 2.5. Effects of a substrate analogue on NAD-ME1 kinetic and regulatory properties

Oxaloacetate (OAA) is an L-malate analogue that was shown to activate NAD-ME1 (Tronconi et al., 2010b). The response observed in L-malate curves as a consequence of increasing the OAA levels was a decrease in the $n_H$ values (Fig. 6A), reaching a hyperbolic response ($n_H$ = 1.0) at 1 mM OAA. No significant modifications in the $k_{cat}$ and $K_{0.5}$ for L-malate values were observed in the presence of OAA (Fig. 6A). Thus, OAA only suppresses the sigmoidal behavior of L-malate saturation curves of NAD-ME1.

On the other hand, the initial rate of NAD-ME1 was evaluated as function of increasing concentrations of OAA and fumarate, at a fixed and suboptimal L-malate concentration (Fig. 6B and C). When the data are represented as a function of fumarate concentration, increasing OAA levels produced a decrease in the fumarate activation effect on NAD-ME1 activity (Fig. 6B). Conversely, upon varying OAA concentration, a hyperbolic decay of NAD-ME1 activity was observed when the fumarate concentration was higher than 1 mM (Fig. 6C). At high OAA levels, a plateau (approximately 200% activation) was reached regardless of the presence of fumarate. These results indicate antagonistic effects between fumarate and OAA on NAD-ME1 activity due to a competition for the binding to the allosteric site. It is worth mentioning that none of the NAD-ME1 mutant proteins characterized (R50A, R80A and R84A) were activated by OAA (data not shown).

## 3. Discussion

### 3.1. L-Malate binds to NAD-ME1 allosteric site modifying the kinetic behaviour and substrate affinity

The aim of this work was to analyze the possible structural connections between sigmoidal L-malate response and fumarate allosteric regulation of Arabidopsis mitochondrial NAD-ME1. The first clues came from NAD-ME1 L-malate kinetic behavior in the presence of fumarate (Fig. 1). This acid activates NAD-ME1 by decreasing the $K_{0.5}$ value for L-malate without modifying the $k_{cat}$ value (Table 1). What is even more important is that fumarate decreases the $n_H$ value and, at 4 mM of modulator, the L-malate saturation curve is hyperbolic (Fig. 1). These results suggest that this substrate is also binding to an exosite generating the sigmoidal kinetic behavior exhibited by NAD-ME1. Fumarate could compete with L-malate by the exosite and, at elevated concentrations, change the saturation curve to a hyperbolic one. More evidence is obtained from the analysis of chimeric proteins of NAD-ME1 and -2. The replacement of the amino region in NAD-ME1q and -2q interchanged both properties in this study, as NAD-ME2q gained a sigmoidal L-malate response and fumarate activation while NAD-ME1q lost the aforementioned characteristics (Fig. 1). This aminoacidic region was previously determined as being responsible for fumarate activation in NAD-ME1 (Tronconi et al., 2010b). Thereby, the L-malate exosite could actually be a fumarate allosteric site. However, kinetic data are not conclusive and a cooperative effect between active sites in the dimer that is affected by fumarate binding to NAD-ME1 could also be taking place.

Thus, a series of quenching of intrinsic fluorescence assays using L-malate were performed. L-Malate is a very weak dynamic quencher as its $K_d$ for free tryptophan is two orders of magnitude lower than the value obtained for fumarate (Suppl. Fig. 1) (Tronconi et al., 2012). Thereby, contrary to fumarate, that acts both as a collisional and a static quencher of EM-NAD1 and -2 fluorescence (Tronconi et al., 2012), L-malate only quenches through a static process that involves the binding of the acid to the protein. Contrary to NAD-ME2, which exhibits a single phase curve Stern–Volmer representation, NAD-ME1 shows biphasic curves (Suppl. Fig. 1). These results indicate that NAD-ME1 actually presents two binding sites for L-malate: the active site required for the catalysis and a second allosteric regulatory site, with a different L-malate affinity (Table 2), that is absent in NAD-ME2 (Fig. 2). In the absence of NAD, the $K_D$ value for L-malate of NAD-ME1 active site ($K_{D2}$) was 28-fold higher than the $K_D$ value of the extra site ($K_{D1}$) in NAD-ME1 (Table 2).

The quenching fluorescence assays performed on NAD-ME1q and -2q proteins provide independent evidence that the L-malate exosite is located at the amino-terminal region of NAD-ME1. The

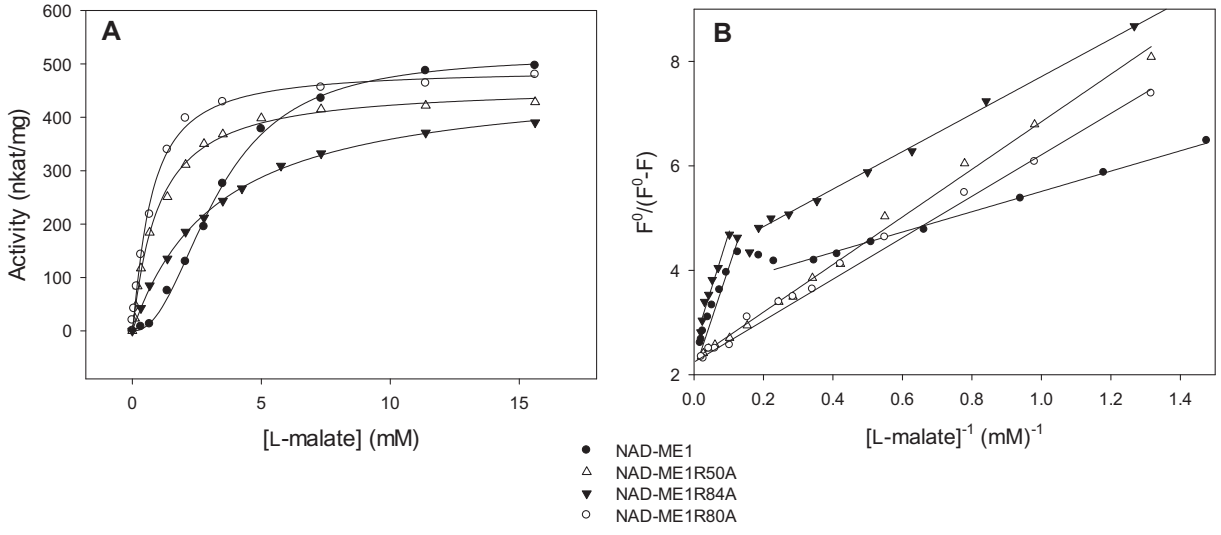


**Fig. 5.** Kinetic and quenching properties of NAD-ME1 mutants. (A) Enzymatic activity was determined for mutant proteins R50A, R84A and R80A using L-malate as variable substrate. Assays were done at 4 mM NAD and 10 mM $MnCl_2$. Typical results are shown from at least three independent determinations. For comparison, kinetic L-malate curve for NAD-ME1 is shown. (B) Modified Stern–Volmer representations of L-malate quenching data for R50A, R84A and R80A are shown. The excitation wavelength was set at 295 nm and the fluorescence was recorded at 344 nm. All values were corrected for buffer spectra and dilution. For comparison, quenching L-malate curve for NAD-ME1 is shown. The quenching constants are summarized in Table 2.

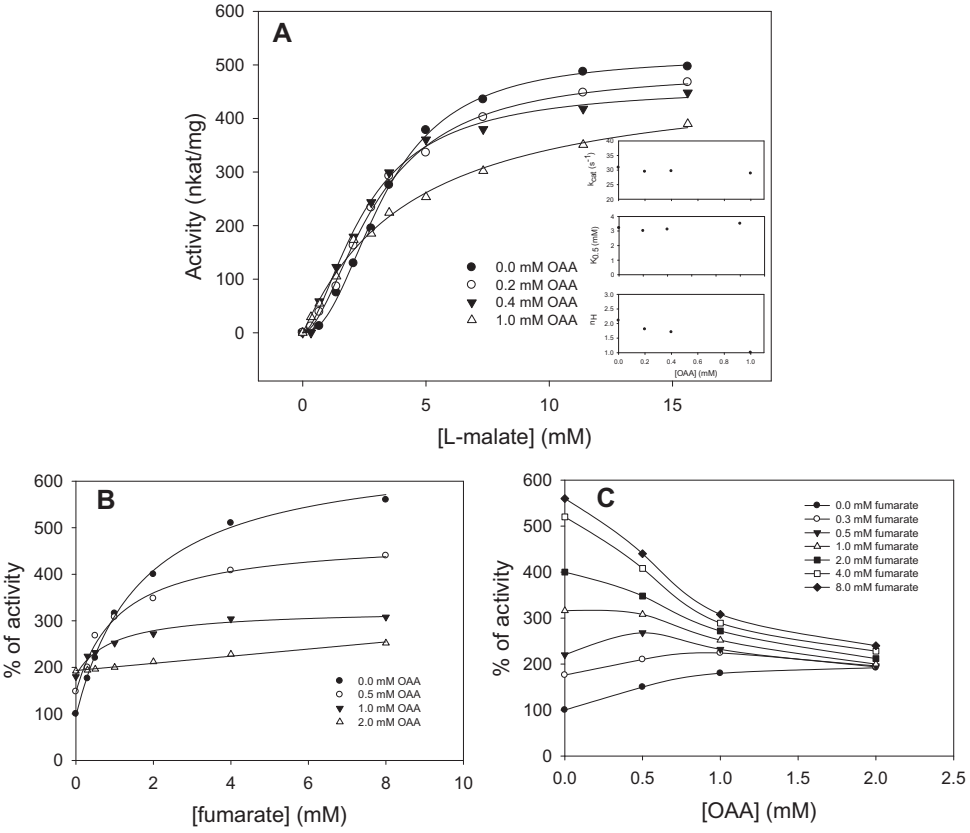


**Fig. 6.** Effect of OAA on NAD-ME1 activity. (A) Enzymatic activity was determinated using L-malate as variable substrate and 4 mM NAD at different levels of OAA. The values of $n_H$, $K_{0.5}$ and $k_{cat}$ obtained as function of OAA concentration are shown as inset. Enzymatic activity was determinated using 0.7 mM L-malate and 4 mM NAD at different concentration of fumarate and OAA. Results presented as the% of activity in the presence of both metabolites in relation to the activity measured in the absence of them, representing as variable fumarate (B) or OAA (C).

loss of the exosite in NAD-ME1q was accompanied by a significant increase of substrate affinity for the active site in comparison to the parental enzymes (Table 2). This agrees with our kinetic data, as NAD-ME1q showed a 15-fold lower $K_{0.5}$ for L-malate than NAD-ME1 or -2 (Table 1). On the other hand, NAD-ME2q gained the exosite by the aminoacidic replacement and this provoked a non-hyperbolic kinetic response, proving that both characteristics are linked. Moreover, the $K_{D1}$ value for NAD-ME2q is similar to the $K_{D1}$ value for NAD-ME1 (Table 2). This result implies that the conformation of the exosite was not considerably altered by the aminoacidic interchange and thus the amino region of NAD-ME1 contains all the structural elements needed for the constitution of a correct exosite.

In the presence of fumarate, NAD-ME1 S–V plot for L-malate quenching changed its biphasic behavior to single phase one, implying that the substrate only binds to one site (Fig. 3B). Also, the affinity of fumarate binding to NAD-ME1 is decreased by the presence of L-malate (Fig. 3A). These results clearly indicate that L-malate and fumarate compete for the binding to the same site and demonstrate that the L-malate exosite identified in this work corresponds to the fumarate site previously described (Tronconi et al., 2012). In addition, in the presence of fumarate, the affinity of NAD-ME1 active site for L-malate is increased, which is consistent with the data obtained by kinetic approaches (Table 1).

Characterization of NAD-ME1 mutant proteins with aminoacidic substitutions in the allosteric site provides further information regarding L-malate and fumarate binding. Three residues that belong to the allosteric site were identified (Fig. 4), although each one contributes differently to $C_4$ organic acid binding. The R50A protein is a hyperbolic and non-fumarate activated enzyme, as neither L-malate nor fumarate binds at the allosteric site (Fig. 5B and Suppl. Fig. 2). This protein showed higher affinity for L-malate in the active site with a $K_D$ value 2-fold lower than the parental enzyme (Table 2). This resulted in a decrease of about 7-fold of the $K_{0.5}$ L-malate kinetic value (Fig. 5A, Table 1). These results are similar to those obtained when the allosteric site was completely removed in NAD-ME1q or when fumarate binds to parental NAD-ME1 (Table 1). Thus, L-malate binding at the exosite not only changes NAD-ME1 kinetic behavior, but also decreases the affinity of the active site for this substrate. In addition, the heterotrophic activation effect of fumarate is a consequence of the displacement of L-malate from the allosteric site. Hence, fumarate is not really an activator but is in fact a suppressor of the inhibitory effect of L-malate on NAD-ME1.

The properties exhibited by the other mutant protein, R80A, support this idea. R80A is a non-hyperbolic enzyme (Fig. 5A) with a higher affinity for L-malate at the active site than parental NAD-ME1 (Table 1 and 2). L-Malate cannot bind at the allosteric site (Fig. 5B), but this protein can still bind fumarate (Suppl. Fig. 2). However, its catalytic efficiency is marginally increased by fumarate in comparison to the parental enzyme (Table 1). Again, the loss of L-malate binding at the allosteric site generates a high substrate affinity enzyme. Arg80 is involved in L-malate binding to the allosteric site but not in fumarate binding to this site.

Finally, mutant R84A is also a non-allosteric enzyme, as for R50A (Fig. 5A and Suppl. Fig. 2). However, while fumarate is not able to bind to this protein (Suppl. Fig. 2), L-malate does bind to the allosteric site, but with decreased affinity (Table 2). The 5-fold

higher $K_{D1}$ value of R84A results in a hyperbolic response with a $K_{0.5}$ for L-malate similar to the one of the parental NAD-ME1 (Table 1). Thereby, Arg84 is critical for fumarate binding, as was previously proved for this enzyme (Tronconi et al., 2012) but has a minor role in L-malate binding.

The kinetic assays also indicated that OAA abolished the L-malate sigmoidal response (Fig. 6A) and neutralized the fumarate effect (Fig. 6B and C). Hence, OAA could bind at the NAD-ME1 allosteric site and act as L-malate by decreasing the substrate affinity at the active site.

$C_4$ organic acid regulation was also reported for the mitochondrial NAD-ME from *A. suum*. For this isoform, both L-malate and fumarate act as activators, binding to different allosteric sites (Karsten et al., 2003). However, Arabidopsis NAD-ME1 is oppositely regulated by these acids through the binding of these molecules to the same regulatory site. The presence of the conserved Arg80, which is exclusively involved in L-malate binding in plant isoforms (Fig. 4A), could be a structural determinant for the differences observed between animal and plant NAD-MEs.

### 3.2. Fumarate and/or L-malate as in vivo allosteric effectors of NAD-ME1

*A. thaliana* can accumulate great amounts of L-malate and fumarate with extremely variable levels depending on the tissue, the plant's age, and the growth conditions (Araújo et al., 2011; Fernie and Martinoia, 2009). Although no data are available on mitochondrial organic acid concentrations, homo and heterotrophic regulatory effects may occur *in vivo* in NAD-ME1, taking into account the comparable $K_D$ values for the allosteric site obtained for each ligand (0.4 mM for L-malate and 1.4 mM for fumarate).

In this plant, both acids exhibit a diurnal accumulation profile, reaching a maximum at the end of the light period (Pracharoenwattana et al., 2010). At night, both compounds are used to replenish TCA intermediates and/or respiration through the enhanced NAD-ME activity that takes place during this period (Tronconi et al., 2008). Despite their structural homologies, specific functions can be proposed for each $C_4$ acid. Contrary to fumarate, L-malate is a powerful reducing agent and its accumulation must be strictly regulated to avoid redox unbalances (Centeno et al., 2011). Thereby, fumarate is a suitable carbon signal molecule as its concentration can greatly fluctuate without greatly affecting redox homeostasis. The subcellular location of fumarate in plant cells is unknown, but it could be accumulated in the vacuole, as L-malate. However, taking into account that the cytosolic fumarase RNA abundance and mitochondrial fumarase activity in Arabidopsis leaves are higher in light than in the dark (Gibon et al., 2004; Lee et al., 2010), it can be assumed that in this species fumarate can be accommodated to some extent in the cytosol and mitochondria during the day.

The results of this study indicate that the affinity of L-malate for the exosite in NAD-ME1 is greater than its affinity for the active site (Table 2). In addition, the presence of L-malate at the NAD-ME1 allosteric site generates a low affinity enzyme (Table 1). Thus, in Arabidopsis, high NAD-ME1 activity is reached when L-malate levels are elevated in mitochondria, as observed when it is necessary to dissipate redox power imported from other subcellular compartments in the form of L-malate (Fig. 7A; Fernie and Martinoia, 2009). On the other hand, when fumarate levels increase at the end of each period of light in Arabidopsis leaves, NAD-ME1 becomes a high substrate-affinity enzyme by the displacement of L-malate from the allosteric site. Under this situation, NAD-ME1 could be working in coordination with mitochondrial and/or cytosolic fumarase for nocturnal respiration of large fumarate reserves (Fig. 7B).

### 3.3. Allosteric transmission signal is present in NAD-ME2

The replacement of the amino-terminal region in NAD-ME2q produced a sigmoid and fumarate-activated enzyme due to the gain of the allosteric site. L-Malate binding at this site changes the kinetic response to a non-hyperbolic one (Fig. 1) and decreases substrate affinity at the active site in comparison to NAD-ME2 (Table 1). In addition, as in NAD-ME1, fumarate binding releases the enzyme from substrate inhibition (Fig. 1D; Table 1). Thus, the communication of the allosteric signal between effector and active site was maintained in NAD-ME2q. This is an important fact, as allosteric proteins have evolved to have a significantly higher extent of very specific quaternary and tertiary motions than their non-allosteric counterparts (Daily and Gray, 2007). Usually, theses

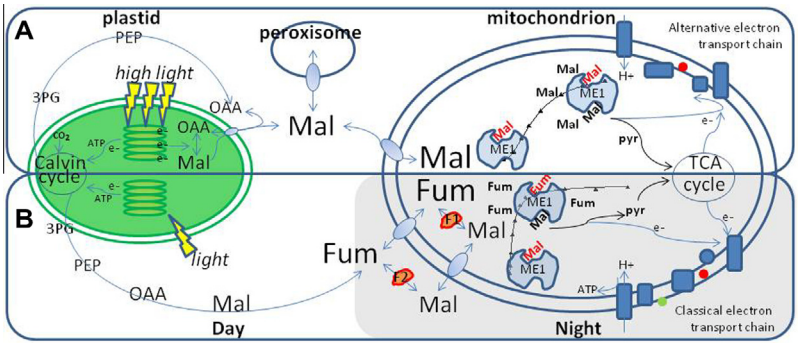


**Fig. 7.** Hypothetical model of NAD-ME1 function in Arabidopsis metabolism. (A) Under photorespiratory conditions reducing equivalents are exported from mitochondria by L-malate-OAA shuttle to support hydroxypyruvate reduction in peroxisomes. In this case, NAD-ME1 should exhibit a marginal activity because the enzyme is set in the low substrate affinity form (as L-malate is present at the allosteric site) and the low L-malate levels in this compartment. However, the over reduction of chloroplasts (eg. by high light) increases L-malate/OAA ratio that force the uptake of L-malate by mitochondria (Backhausen et al., 1994; Padmasree et al., 2002). The high levels of this acid in mitochondria could be metabolized by the low affinity form of NAD-ME1 and NAD-ME2 to dissipate the excess of reducing equivalents through alternative – non phosphorylating – pathway of electron transport (Padmasree et al., 2002). (B) Arabidopsis leaves accumulate exceptionally high fumarate levels at the end of each light period (Chia et al. 2000). During the night, this acid is mobilized to replenish the TCA cycle intermediates pool and to supply carbon for mitochondrial respiration through classical – phosphorylating – pathway. Such processes require the concerted action of cytosolic and/or mitochondrial fumarase and NAD-ME1, which could become a high substrate affinity enzyme as fumarate replaced L-malate at the allosteric site. Hence, L-malate do not need to be accumulated at high levels to be metabolized by NAD-ME1. Under this scenario, NAD-ME2 activity would be very low, as this isoform is competitively inhibited by fumarate (Tronconi et al., 2012). F1 and F2: mitochondrial and cytosolic fumarases present in Arabidopsis, respectively. 3PG: 3-phosphoglycerate, PEP: phosphoenolpyruvate, OAA: oxaloacetate, Mal: L-malate, Fum: fumarate. e-: reducing equivalents. ME1: NAD-ME1. In ME1, top and bottom cavities represent the allosteric and active sites, respectively. Functional enzyme is indicated by pyruvate (pyr) generation. The letter size of Mal and Fum is in relation to the relative level of such metabolites in the compartments.

motions are mechanically coupled at distances of up to 20 Å, enough to bridge allosteric and active sites and to cross domains and subunits (Daily and Gray, 2009). Thus, parental NAD-ME2 possesses the ability to transmit the effector signal in its structure despite not being able to bind neither fumarate nor L-malate. The presence of the Arg triad (R50, R80 and R84) in NAD-ME2 (Fig. 4A) suggests that this isoform could once be modulated by these acids but later evolved to acquire new regulatory and kinetic properties for its particular specificity of function (Tronconi et al., 2010b).

## 4. Concluding remarks

Allosteric regulation is a major mechanism of control in many biological processes, including cell signaling, gene regulation and metabolic flux (Carrari et al., 2006; Gibon et al., 2004; Kümmel et al., 2006; Steinhauser et al., 2010). Thus, comprehension of its mechanisms is critical for the understanding of such processes. The results presented here clearly indicate that fumarate and L-malate bind to the same regulatory site in Arabidopsis NAD-ME1. Residues Arg50, Arg80 and Arg84 of NAD-ME1 were shown to have different participations in L-malate and fumarate binding at the allosteric site. These residues form a triad, which is the basis of the homo and heterotrophic effects that characterize NAD-ME1. In addition, fumarate is not a true activator but releases NAD-ME1 from L-malate inhibition. This complex regulation has not been reported for any malic enzyme characterized to date and clearly indicates an important role of this enzyme controlling the flow of $C_4$ organic acids in plant mitochondrial metabolism.

## 5. Experimental

### 5.1. Site-directed mutagenesis of NAD-ME1

Site-directed mutagenesis of NAD-ME1 was carried out according to the procedure described by Mikaelian and Sergeant (1992). Briefly, the pENTR/D-TOPO plasmid containing the NAD-ME1 cDNA insert (Tronconi et al., 2008) was used as PCR template to amplify a fragment of about 270 bp using the following primers:

NAD-ME1 for: 5′-GGATCCCCCACCATCGTTCATAAA-3′ (Tronconi et al., 2008)
R50A: 5′- GTCATAAA**GC**AAAAATCTG-3′
R80A: 5′-CATGTAACG**C**ATTAAGAATCC-3′

in which the position of the mutation is highlighted and the codon which was changed is underlined in the oligonucleotide sequence. The PCR was carried out using a mixture of *Taq* and *Pfu* polymerases (10:1) in order to reduce possible mistakes introduced by *Taq* polymerase. The fragment containing the mutation was purified from the PCR mix and used as a primer to amplify the full sequence using the pENTR/D-TOPO as template and the primer NAD-ME1rev: 5′-GTCTACAAGGATGACTAAGTCGAC-3′ (Tronconi et al., 2008). After cloning in the pET32 vector, the fragment was sequenced to verify the introduction of the corresponding mutation and that no undesired modifications were added during PCR and cloning procedures.

### 5.2. Heterologous expression and purification of the recombinant enzymes

The pET32 vectors containing the inserts encoding for NAD-ME1, NAD-ME2 (Tronconi et al., 2008), NAD-ME1q and NAD-ME2q (Tronconi et al., 2010b), NAD-ME1R84 (Tronconi et al., 2012), NAD-ME1R50 and NAD-ME1R80 (this work) were used to express each NAD-ME fused in frame to a His-tag to be purified by a nickel containing His-binding column (Novagen). The induction in *Escherichia coli* BL21(DE3) cells and the purification of the proteins were performed as previously described (Tronconi et al., 2008). Fusion proteins were digested with 0.8–1.3 nkat of enterokinase (EK-Max; Invitrogen) per milligram of protein at 16 °C for 2 h to remove the N-terminus encoded by the expression vector. The protease was eliminated using EK-Away resin (Invitrogen) according to manufacturer's instructions. The purified enzymes were concentrated on Centricon YM-50 (Amicon), analyzed by SDS–PAGE to verify integrity and purity and stored at −80 °C for further studies in 50 mM Mes-NaOH pH 6.5, 5 mM $MnCl_2$, 5 mM DTT and 50% (v/v) glycerol.

Prior to the fluorescence assays, the concentrated proteins were changed to a buffer composed by 50 mM Mes-NaOH pH 6.5 and 3 mM $MnCl_2$ using a Centricon YM-50 device (Amicon).

### 5.3. Activity assays and protein concentration measurement

The oxidative decarboxylation of L-malate was assayed spectrophotometrically using a reaction mixture containing 50 mM Mes-NaOH pH 6.5, 10 mM $MnCl_2$, NAD and L-malate in a final volume of 0.5 ml. The reaction was started by the addition of L-malate. One katal (kat) is defined as the amount of enzyme that catalyzes the formation of 1 mol of NADH per sec under the specified conditions ($\varepsilon_{340nm}$ = 6.22 $mM^{-1}$ $cm^{-1}$).

Initial velocity studies were performed by varying the concentration of one of the substrates around its $K_{0.5}$ value, while keeping the other substrate concentrations at saturating levels. $K_{0.5}$ values for $NAD^+$ and L-malate were again assayed for new stocks of purified NAD-ME1, NAD-ME2, NAD-ME1q, NAD-ME2q and NAD-ME1R84A (Tronconi et al., 2012, 2010b, 2008). All kinetic parameters were calculated at least in triplicate and adjusted to non-linear regression using free concentrations of all substrates (Tronconi et al., 2010a). The substrate dependent rates were fitted to the Michaelis–Menten or the Hill equations.

When testing the ability of fumarate or oxalacetate (OAA) as modulators of the enzymatic activity, NAD-ME activity was measured in the absence and presence of different concentrations of these metabolites (0–10 mM).

All activity assays were carried out at 30 °C in a Helios $\beta$ spectrophotometer (Unicam). Protein concentration was determined by the BioRad Protein Assay with total serum protein as standard.

### 5.4. Gel electrophoresis

SDS–PAGE was performed in 8–10% (w/v) polyacrylamide gels according to Laemmli (1970). Proteins were visualized with Coomassie blue or electroblotted onto a nitrocellulose membrane for immunoblotting. Either anti NAD-ME1 or anti NAD-ME2 antibodies (Tronconi et al., 2008) were used for detection. Bound antibodies were visualized by linking to alkaline phosphatase-conjugated goat anti-rabbit IgG according to the manufacturer's instructions (Sigma). Alkaline phosphatase activity was detected colorimetrically.

### 5.5. Fluorescence titration

Fluorescence data were collected in a Cary Eclipse fluorescence spectrophotometer, using quartz cuvettes with an inner volume of 0.75 ml. The excitation wavelength was set to 295 nm to selectively excite tryptophan and the fluorescence emission was recorded at 344 nm (Tronconi et al., 2012). The titration was carried out by sequentially adding small volumes of either a 500 mM L-malate or 100 mM fumarate stock solution. All data were gathered at 50 mM Mes-NaOH pH 6.5, 3 mM $MnCl_2$ with

5–8 μmol of enzyme (or 50 μM of free tryptophan). Buffer fluorescence was recorded and subtracted from sample data. Fluorescence intensity was corrected for dilution resulting from the addition of L-malate or fumarate.

The quenching data obtained by varying L-malate or fumarate concentration were represented in the form of the Stern–Volmer equation:

$$F^0/F = 1 + \mathrm{K} * [\mathrm{Q}] \quad (1)$$

where the amount of fluorescence measured is represented as $F^0/F$, being $F^0$ the fluorescence of the enzyme (or free tryptophan) alone and $F$ the fluorescence of the enzyme (or free tryptophan) in the presence of quencher. [Q] is the quencher concentration and $K$ is the constant $K_d$ (dynamic constant) or $K_A$ (thermodynamic association constant) for dynamic or static quenching, respectively. Dynamic quenching occurs by collision between the quencher and the fluorophore (free tryptophan or protein). Instead, the static decay process implicates that the quencher binds to the protein and allows the calculation of the binding constants. Alternatively, when the data were downwardly curved, they were analyzed in terms of the modified Stern–Volmer equation (Lehrer and Leavis, 1978), which allows the discrimination between accessible and inaccessible tryptophan residues:

$$F^0/(F^0 - F) = 1/\mathrm{fa} * \mathrm{K} * [\mathrm{Q}] + 1/\mathrm{fa} \quad (2)$$

where fa is the fraction of fluorophores available to the quencher. Under static quenching, the dissociation constant ($K_D$) for the quencher-enzyme complex was calculated as $1/K_A$.

Alternatively, quenching data were also analyzed by fitting to the Langmuir isotherm equation for one (Eq. (3)) or two binding site (Eq. (4)) (Hays et al., 2004):

$$(F^0 - F)/F^0 = [\mathrm{Q}]/(\mathrm{K_D} + [\mathrm{Q}]) \quad (3)$$

$$(F^0 - F)/F^0 = [\mathrm{Q}]/(\mathrm{K_{D1}} + [\mathrm{Q}]) + [\mathrm{Q}]/(\mathrm{K_{D2}} + [\mathrm{Q}]) \quad (4)$$

The equation that gave the lowest standard errors was assumed to represent the model that best describes the quencher binding to the enzyme. All determinations were performed at least in triplicate with $K_D$ values no more different than 5% S.D.

## Acknowledgements

The authors thank Alejandro Vila's group at the Rosario Molecular Biology Institute for kindly facilitating the use of spectrofluorometer. MAT, MCGW, CSA and MFD are members of the Researcher Career of the National Council of Scientific and Technical Research (CONICET). This work has been financially supported by the National Agency for Scientific and Technological Promotion [PICT 2007-1452; PICT 2010-2078; PICT 2164] and CONICET [PIP 00766].

## Appendix A. Supplementary data

Supplementary data associated with this article can be found, in the online version, at http://dx.doi.org/10.1016/j.phytochem.2014.11.009.

## References

Araújo, W.L, Nunes-Nesi, A., Fernie, A.R., 2011. Fumarate: multiple functions of a simple metabolite. Phytochemistry 72, 838–843.

Arias, C.L., Andreo, C.S., Drincovich, M.F., Gerrard Wheeler, M.C., 2013. Fumarate and cytosolic pH as modulators of the synthesis or consumption of $C_4$ organic acids through NADP-malic enzyme in *Arabidopsis thaliana*. Plant Mol. Biol. 81, 297–307.

Backhausen, J.E., Kitzmann, C., Scheibe, R., 1994. Competition between electron acceptors in photosynthesis: regulation of the malate valve during $CO_2$ fixation and nitrite reduction. Photosynth. Res. 42, 75–86.

Carrari, F., Baxter, C., Usadel, B., Urbanczyk-Wochniak, E., Zanor, M.I., Nunes-Nesi, A., Nikiforova, V., Centero, D., Ratzka, A., Pauly, M., Sweetlove, L.J., Fernie, A.R., 2006. Integrated analysis of metabolite and transcript levels reveals the metabolic shifts that underlie tomato fruit development and highlight regulatory aspects of metabolic network behavior. Plant Physiol. 142, 1380–1396.

Centeno, D.C., Osorio, S., Nunes-Nesi, A., Bertolo, A.L.F., Carneiro, R.T., Araújo, W.L., Steinhauser, M.C., Michalska, J., Rohrmann, J., Geigenberger, P., Oliver, S.N., Stitt, M., Carrari, F., Rose, J.K.C., Fernie, A.R., 2011. Malate plays a crucial role in starch metabolism, ripening, and soluble solid content of tomato fruit and affects postharvest softening. Plant Cell 23, 162–184.

Chia, D.W., Yoder, T.J., Reiter, W.D., Gibson, S.I., 2000. Fumaric acid: an overlooked form of fixed carbon in Arabidopsis and other plant species. Planta 211, 743–751.

Daily, M. D, Gray, J. J, 2009. Allosteric communication occurs via networks of tertiary and quaternary motions in proteins. PLoS Comput Biol. 5, e1000293.

Daily, M.D., Gray, J.J., 2007. Local motions in a benchmark of allosteric proteins. Proteins 67, 385–399.

Fernie, A.R., Martinoia, E., 2009. Malate. Jack of all trades or master of a few? Phytochemistry 70, 828–832.

Gerrard Wheeler, M.C., Arias, C.L., Tronconi, M.A., Maurino, V.G., Andreo, C.S., Drincovich, M.F., 2008. *Arabidopsis thaliana* NADP-malic enzyme isoforms: high degree of identity but clearly distinct properties. Plant Mol. Biol. 67, 231–242.

Gibon, Y., Blaesing, O.E., Hannemann, J., Carillo, P., Höhne, M., Hendriks, J.H.M., Palacios, N., Cross, J., Selbig, J., Stitt, M., 2004. A robot-based platform to measure multiple enzyme activities in Arabidopsis using a set of cycling assays: comparison of changes of enzyme activities and transcript levels during diurnal cycles and in prolonged darkness. Plant Cell 16, 3304–3325.

Hanning, I., Heldt, H.W., 1993. On the function of mitochondrial metabolism during photosynthesis in spinach (*Spinacia oleracea* L.) leaves. Partitioning between respiration and export of redox equivalents and precursors for nitrate assimilation products.. Plant Physiol. 103, 1147–1154.

Hays, M.D., Ryan, D.K., Pennell S., 2004. A modified multisite Stern–Volmer equation for the determination of conditional stability constants and ligand concentrations of soil fulvic acid with metal ions. Anal. Chem. 76, 848–854.

Jiang, P., Du, W., Mancuso, A., Wellen, K.E., Yang, X., 2013. Reciprocal regulation of p53 and malic enzymes modulates metabolism and senescence. Nature 493, 689–693.

Karsten, W.E., Pais, J.E., Rao, G.S.J., Harris, B.G., Cook, P.F., 2003. *Ascaris suum* NAD-malic enzyme is activated by malate and fumarate binding to separate allosteric sites. Biochemistry 42, 9712–9721.

Kümmel, A., Panke, S., Heinemann, M., 2006. Systematic assignment of thermodynamic constraints in metabolic network models. BMC Bioinformatics 23, 512.

Laemmli, U.K., 1970. Cleavage of structural proteins during the assembly of the head of bacteriophage T4. Nature 227, 680–685.

Lehrer, S.S., Leavis, P.C., 1978. Solute quenching of protein fluorescence. Methods Enzymol. 49, 222–236.

Lee, C.P., Eubel, H., Millar, A.H., 2010. Diurnal changes in mitochondrial function reveal daily optimization of light and dark respiratory metabolism in Arabidopsis. Mol. Cell Proteomics 9, 2125–2139.

Mallick, S., Harris, B.G., Cook, P.F., 1991. Kinetic mechanism of NAD: malic enzyme from*Ascaris suum* in the direction of reductive carboxylation. J. Biol. Chem. 266, 2732–2738.

Mikaelian, I., Sergeant, A., 1992. A general and fast method to generate multiple site directed mutations. Nucleic Acids Res. 20, 376.

Moreadith, R.W., Lehninger, A.L., 1984. Purification, kinetic behavior, and regulation of NAD(P)1 malic enzyme of tumor mitochondria. J. Biol. Chem. 259, 6222–6227.

Padmasree, K., Padmavathi, L, Raghavendra, A.S., 2002. Essentiality of mitochondrial oxidative metabolism for photosynthesis: optimization of carbon assimilation and protection against photoinhibition. Crit. Rev. Biochem. Mol. Biol. 37 (2), 71–119.

Pracharoenwattana, I., Zhou, W.X., Keech, O., Francisco, P.B., Udomchalothorn, T., Tschoep, H., Stitt, M., Gibon, Y., Smith, S.M., 2010. Arabidopsis has a cytosolic fumarase required for the massive allocation of photosynthate into fumaric acid and for rapid plant growth on high nitrogen. Plant J. 62, 785–795.

Rao, G.S.J., Coleman, D.E., Karsten, W.E., Cook, P.F., Harris, B.G., 2003. Crystallographic studies on *Ascaris suum* NAD-malic enzyme bound to reduced cofactor and identification of an effector site. J. Biol. Chem. 278, 38051–38058.

Steinhauser, M.C., Steinhauser, D., Koehl, K., Carrari, F., Gibon, Y., Fernie, A.R., Stitt, M., 2010. Enzyme activity profiles during fruit development in tomato cultivars and *Solanum pennellii*. Plant Physiol. 153, 80–98.

Sweetlove, L.J., Beard, K.F.M., Nunes-Nesi, A., Fernie, A.R., Ratcliffe, R.G., 2010. Not just a circle: flux modes in the plant TCA cycle. Trends Plant Sci. 15, 462–470.

Tronconi, M.A., Gerrard Wheeler, M.C., Drincovich, M.F., Andreo, C.S., 2012. Differential fumarate binding to Arabidopsis NAD+ malic enzymes 1 and -2 produces an opposite activity modulation. Biochimie 94, 1421–1430.

Tronconi, M.A., Gerrard Wheeler, M.C., Maurino, V.G., Drincovich, M.F., Andreo, C.S., 2010a. NAD-malic enzymes of *Arabidopsis thaliana* display distinct kinetic mechanisms that support differences in physiological control. Biochem. J. 430, 295–303.

Tronconi, M.A., Maurino, V.G., Andreo, C.S., Drincovich, M.F., 2010b. Three different and tissue-specific NAD-malic enzyme generated by alternative subunit association in *Arabidopsis thaliana*. J. Biol. Chem. 285, 11870–11879.

Tronconi, M.A., Fahnenstich, H., Gerrard Wheeler, M.C., Andreo, C.S., Flügge, U.I., Drincovich, M.F., Maurino, V.G., 2008. Arabidopsis NAD-malic enzyme functions as a homodimer and heterodimer and has a major impact during nocturnal metabolism. Plant Physiol. 146, 1540–1552.

Willeford, K.O., Wedding, R.T., 1987. Evidence for a multiple subunit composition of plant NAD malic enzyme. J. Biol. Chem. 262, 8423–8429.

Yang, Z., Lanks, C.W., Tong, L., 2002. Molecular mechanism for the regulation of human mitochondrial NAD(P)+ dependent malic enzyme by ATP and fumarate. Structure 10, 951–960.